Effects of Random Perturbations in Plastic Optical Fibers

A. F. Garito, J. Wang, R. Gao

REVIEW

The most important feature of an optical fiber waveguide is its bandwidth, which defines its information-carrying capacity. A major limitation on the bandwidth of multimode glass and plastic optical fibers is modal dispersion, in which different optical modes propagate at different velocities and the dispersion grows linearly with length. However, in plastic optical fibers, experimental and theoretical results indicate that the modes are not independent but are highly coupled, which leads to a characteristic square-root length dependence and an unanticipated large enhancement of the bandwidth to gigahertz levels. The ever increasing demands for low-cost, high-bandwidth communications media for voice, video, and data transmission in short- and medium-distance applications are generating a new assessment of multimode optical fibers to serve as high-speed fiber links.

Optical communication systems based on glass optical fibers (GOFs) allow communication signals to be transmitted not only over long distances with low attenuation but also at extremely high data rates, or bandwidth capacity. This capability arises from the propagation of a single optical signal mode in the low-loss windows of glass located at the near-infrared wavelengths of 0.85, 1.3, and 1.55 μm. Since the introduction of erbium-doped fiber amplifier (EDFA), the last decade has witnessed the emergence of single-mode GOF as the standard data transmission medium for wide area networks (WANs), especially in terrestrial and transoceanic communication backbones. In addition, the bandwidth performance of single-mode GOF has been vastly enhanced by the development of dense wavelength division multiplexing (DWDM), which can couple up to 40 channels of different wavelengths of light (colors) into a single fiber, with each channel carrying gigabits of data per second. Moreover, in a recent demonstration by Lucent Technologies, signal transmission of 1 terabit (10^{12} bits) per second was achieved over a single fiber on a 100-channel DWDM system. Enabled by these and other technologies, the bandwidth capacities of the communication networks are increasing at rates of as much as an order of magnitude per year.

The success of the single-mode GOF in long-haul communication backbones has given rise to the concept of optical networking, which is a central theme currently driving research and development activities in the field of photonics. The main objective is to integrate voice, video, and data streams over all-optical systems as communication signals make their way from WANs down to smaller local area networks (LANs), and eventually to the end user by fiber to the desktop (FTTD). Examples are the recent explosion of the Internet and use of the World Wide Web, which are demanding vastly higher bandwidth performance in short- and medium-distance applications. However, the single-mode GOF core is typically only a few micrometers in diameter. Yet as the optical network nears the end user starting at the LAN stage, the system is characterized by numerous connections, splices, and couplings that make the use of thin single-mode GOF impractical. Current solutions depend on multimode GOF with a larger core diameter (typically 50 or 62.5 μm) to ease these fiber connection and systems installation issues. However, the increased fiber diameter is accompanied by an increase in the number of optical signal modes to many tens of thousands and consequent optical pulse broadening. The unwanted pulse broadening is due to modal dispersion, in which different modes (light paths) within the fiber carry components of the signals at different velocities, ultimately results in pulse overlap and a garbled communications signal. Additional pulse broadening contributions from wavelength-dependent dispersion (material dispersion) and intramodal (waveguide) dispersion due to the wavelength dependence of the modal group velocity also occur, but to a lesser extent than modal dispersion (*1*). To overcome and compensate for modal dispersion, the refractive index of the fiber core is graded parabola-like from a high index at the fiber core center to a low index in the outer core region, so that the high-order and low-order modes inside the fiber travel at the same group velocity (*2, 3*).

GOF is brittle and fragile at large core diameters; hence, plastic optical fiber (POF) (Fig. 1A) is being seriously considered as a high-bandwidth fiber link for certain short-distance applications because of its ductility and large core diameter (1 mm). Similar to its GOF counterpart, the bandwidth performance of multimode POF is limited by modal dispersion of the signal pulses. This problem can be alleviated by forming graded-index (GI) POF that has a parabola-like index profile.

In this article, we discuss a different approach to overcoming dispersion that also leads to improvements in the bandwidth of POFs. Rather than trying to force all of the modes to travel at the same velocity, we studied the approach of mode coupling, or mode mixing (*4–6*). Recent experiments on POFs in our research group have revealed unanticipated large enhanced bandwidths due to random index perturbations and mode coupling (*7, 8*), which is our main topic here.

Modal dispersion in the optical fiber waveguide is reduced through mode coupling by allowing the energy packets of the input signal pulse to occupy different modes at different times as they are propagating down the waveguide. These conditions can occur by way of random perturbations along the propagation direction of the fiber waveguide. The perturbations induce coupling between the different modes and cause the energy packets to randomly switch modes back and forth, much as automobiles usually interchange lanes during natural traffic flow. In the presence of mode coupling, the modes are no longer independent, and the energy packets in each mode now travel at an averaged group velocity to arrive essentially at the same time at the output end of the waveguide. As a result, the pulse broadening of the output pulse is markedly reduced. With mode coupling, pulse broadening varies only as a characteristic square-root function of the fiber length, as opposed to following a linear dependence (*4–6*). A beautiful example of this characteristic square-root length dependence of pulse broadening is based on a simple random walk model of pulse propagation down a one-dimensional waveguide.

Mode Coupling Models

A light pulse propagating in the fiber consists of many energy packets that are distributed over all guided modes. After a certain waveguide length, or coupling length L_c, has been traversed, the relative energy packet population in each mode no longer changes with propagation

The authors are in the Department of Physics and Astronomy, University of Pennsylvania, Philadelphia, PA 19104, USA.

length. The waveguide system is then in the strongly coupled regime and has established an equilibrium mode distribution (EMD). We consider a fiber of sufficient length $L > L_c$ consisting of n segments, each of length l. This intrinsic length characterizes the coupling strength of the fiber and can be imagined as the mean free path of the energy packets, that is, the average length an energy packet travels in a mode before it is coupled to another guided mode. For convenience, we first use three discrete guided modes, labeled 1, 2, and 3, and will later generalize our results to a large number of modes.

For an energy packet traveling through the fiber, n_i is the number of segments in which the packet stays in mode i, and p_i is the probability that an energy packet is found in mode i under EMD conditions. The group delay time t is then $t = \Sigma_{i=1}^{3} n_i l / v_i$, where v_i is the group velocity associated with mode i. A useful measure of the pulse broadening is the root mean square (rms) width of the group delay time distribution:

$$\sigma = \sqrt{\langle t^2 \rangle - \langle t \rangle^2} \tag{1}$$

Because $\Sigma_{i=1}^{3} n_i = n$ and $\Sigma_{i=1}^{3} p_i = 1$, the average group delay time $\langle t \rangle$ is

$$\begin{aligned} \langle t \rangle &\equiv \sum_{n_1,n_2,n_3} \frac{n!}{n_1! n_2! n_3!} p_1^{n_1} p_2^{n_2} p_3^{n_3} \left(\frac{n_1 l}{v_1} + \frac{n_2 l}{v_2} + \frac{n_3 l}{v_3} \right) \\ &= nl \left(\frac{p_1}{v_1} + \frac{p_2}{v_2} + \frac{p_3}{v_3} \right) \end{aligned} \tag{2}$$

and

$$\begin{aligned} \langle t^2 \rangle &\equiv \sum_{n_1,n_2,n_3} \frac{n!}{n_1! n_2! n_3!} p_1^{n_1} p_2^{n_2} p_3^{n_3} \left(\frac{n_1 l}{v_1} + \frac{n_2 l}{v_2} + \frac{n_3 l}{v_3} \right)^2 \\ &= \left[\sum_{i=1}^{3} \frac{p_i^2 n(n-1) + p_i n}{v_i^2} + 2n(n-1) \sum_{i \neq j} \frac{p_i p_j}{v_i v_j} \right] l^2 \end{aligned} \tag{3}$$

By substituting Eqs. 2 and 3 into Eq. 1, we find that

$$\sigma^2 = Ll \sum_{i,j=1}^{3} p_i p_j \left(\frac{1}{v_i} - \frac{1}{v_j} \right)^2 \tag{4}$$

The result can be generalized to the case of a large total number of discrete modes M:

$$\sigma^2 = Ll \sum_{i,j=1}^{M} p_i p_j \left(\frac{1}{v_i} - \frac{1}{v_j} \right)^2 \tag{5}$$

The above result can be extended to a continuous mode spectrum, where $p(m)$ is the probability distribution function:

$$\sigma^2 = Ll \int\int dm dm' \; p(m) p(m') \left(\frac{1}{v_m} - \frac{1}{v_{m'}} \right)^2 \tag{6}$$

Hence, within the framework of the random walk model for mode coupling, the pulse broadening in the strongly coupled regime is proportional to the square root of the fiber waveguide length.

The types of random perturbations in an optical fiber waveguide can be divided into two classes (*6*). The first class is intrinsic and may include static and dynamic fluctuations, such as the density and concentration fluctuations natural to random glassy polymer materials. The second class is extrinsic variations such as microscopic random bends caused by stress, diameter variations, and fiber core defects such as microvoids, cracks, or dust particles. The perturbation classes can be represented by a general index perturbation $\delta n^2(r,\theta,z) = n^2(r,\theta,z) - n^2(r)$, where $n(r)$ is the ideal index profile and r, θ, and z are cylindrical coordinates representing the radius, azimuthal angle, and distance along the fiber axis, respectively. The power spectrum of the perturbation is then defined as

$$P(r,\theta,\omega) = \left\langle \left| \frac{1}{L} \int_0^L dz \, \exp(i\omega z) \, \delta n^2(r,\theta,z) \right|^2 \right\rangle \tag{7}$$

where L is the fiber length, and the large angle brackets indicate an ensemble average (because the perturbations are random in nature). Coupling between modes i and j can occur only if the ensemble contains perturbations with a spatial frequency component ω such that the following phase-matching condition for the propagation constants β_i and β_j is met (*2*):

$$\omega = |\beta_i - \beta_j| \tag{8}$$

From extensive studies (*5, 6*), mode coupling is found to occur predominantly between adjacent modes because, for most random perturbations, the power spectrum is a strongly decreasing function of ω. For an α-class index profile

$$n(r) = \begin{cases} n_f[1 - 2\Delta(r/a)^\alpha]^{1/2} & \text{for} \quad 0 \leq r \leq a \\ n_c & \text{for} \quad r > a \end{cases} \tag{9}$$

where a is the fiber radius, n_f is the refractive index at the central core, n_c is the refractive index at the cladding region, $\Delta \equiv$

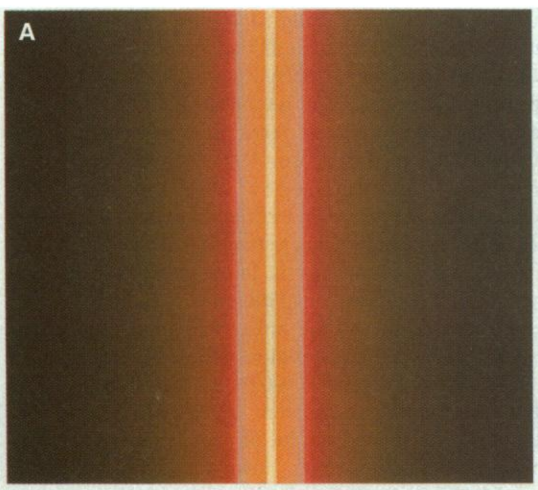

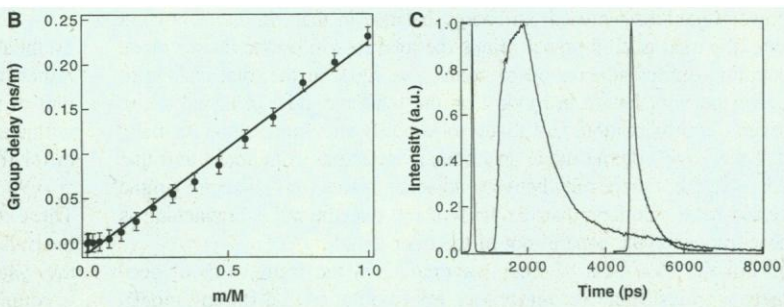

Fig. 1. **(A)** Confocal image of a thickly cladded SI POF sample. The fiber core was doped with fluorescent dye to enhance image resolution. **(B)** Measured differential mode delay profile normalized to length of a 12-m SI POF (dots) as a function of normalized mode number (m/M), which is related to the incidence angle (with respect to the fiber axis) through the relation $m/M = [\sin(\theta)/\sin(\theta_c)]^2$, where θ_c is the acceptance angle of the fiber and least-squares fit (solid line) with slope of 0.24 ± 0.01. The linear dependence of the data indicates a nearly ideal step-like index profile. **(C)** Optical pulses from laser diode light source (left), a 50-m PMMA-based SI POF (middle), and a 100-m PMMA-based GI POF doped with benzyl benzoate (right). The intensity has been normalized. The pulses were offset at different times for illustrative clarity.

$(n_f^2 - n_c^2)/(2n_f^2)$ is the relative index difference, and α is a positive exponent. A step-index profile is a specific case of α-class index profile ($\alpha \rightarrow \infty$). The propagation constant β can be expressed as

$$\beta = n_f k_0 [1 - 2\Delta (m/M)^{\alpha/(\alpha+2)}]^{1/2} \tag{10}$$

where $k_0 = 2\pi/\lambda$ is the free-space wave number, m is the mode ordering number, and M is the total number of guided modes (so that the ratio m/M is the normalized mode number). The number of modes supported by the fiber is given by

$$M = \frac{\alpha}{\alpha + 2} n_f^2 k_0{}^2 a^2 \Delta \tag{11}$$

This yields

$$\delta\beta = \left(\frac{2\alpha}{\alpha + 2}\right)^{1/2} \frac{\sqrt{2\Delta}}{a} \left(\frac{m}{M}\right)^{(\alpha-2)/2(\alpha+2)} \tag{12}$$

Thus, the spectrum that causes mode coupling between guided modes lies in the range

$$\left(\frac{2\alpha}{\alpha + 2}\right)^{1/2} \frac{\sqrt{2\Delta}}{a} \left(\frac{1}{M}\right)^{(\alpha-2)/2(\alpha+2)} \le \omega \le \left(\frac{2\alpha}{\alpha + 2}\right)^{1/2} \frac{\sqrt{2\Delta}}{a} \tag{13}$$

If the perturbation period Λ is defined as

$$\Lambda = \frac{2\pi}{\omega} \tag{14}$$

then Λ is ~9.7 mm for a parabolic GI POF with $a = 250$ μm and $\Delta = 0.013$, and Λ is in the range of 6.2 mm to 10.4 m for a typical cladded step-index (SI) POF with $a = 480$ μm, $\Delta = 0.06$, and $\lambda = 0.65$ μm. For comparison, Λ is ~1.3 mm for a parabolic GI GOF and in the range of 0.9 to 41 mm for a SI GOF with $a = 30$ μm, $\Delta = 0.01$, and $\lambda = 0.65$ μm. In general, for α-class index profiles with α ranging between 2 (parabola) and ∞ (step index), the greater the α value, the wider the Λ spectrum of perturbations that can contribute to mode coupling. In addition, a much wider and longer spectrum of perturbations can appear in a POF because of its larger core diameter relative to glass fibers.

Under mode coupling conditions, the power flow in each mode is governed by the coupled power equation

$$\frac{dP_i}{dz} = \sum_{j=1}^{N} d_{ij}(P_i - P_j) - \gamma_i P_i \tag{15}$$

(*6*), where γ_i is the loss coefficient due to absorption and scattering, P_i is the average power associated with the ith mode, and d_{ij} is the coupling coefficient for a transition between modes i and j. The coupled power equations represent an energy balance in that, on the right-hand side, the total gain in power minus the total loss in power due to mode coupling, minus attenuation of mode i, is equal to the total change in power per unit length in mode i on the left-hand side. In actual cases, several approximations are made to simplify the expression—namely, that the large volume mode spectrum is treated as continuous and that coupling takes place only between adjacent modes (*6*). There are simple closed-form solutions that explicitly show that the pulse broadening is proportional to the square root of the fiber length.

For the case of a SI fiber waveguide, in the framework of geometric optics (that is, under ray approximation), different modes zigzag down the fiber with different propagation angles with respect to the fiber axis. Thus, the mode spectrum can be characterized by the continuous variable θ. Along with the assumption that the coupling coefficient is mode-independent [that is, $d(\theta) \equiv d_0$], Eq. 15 reduces to the following diffusion equation in terms of θ (*6, 9*):

$$\frac{dP(\theta,z)}{dz} = -A\theta^2 P + \frac{D}{\theta}\frac{\partial}{\partial\theta}\left(\theta\frac{\partial P}{\partial\theta}\right) \tag{16}$$

where $P(\theta,z)$ is the angular power distribution, D is the mode conversion coefficient, defined as

$$D = d_0(\lambda/4an_f)^2 \tag{17}$$

and A is the second-order coefficient of the mode-dependent loss coefficient $\gamma(\theta)$, defined as

$$\gamma(\theta) = \gamma_0 + A\theta^2 + \cdots \tag{18}$$

Thus, the coefficients A and D can be experimentally determined directly through simple angle-dependent measurements of the input light.

Mode Coupling in Step-Index Plastic Optical Fibers

There are several different techniques to analyze the bandwidth properties and performance of a multimode optical fiber waveguide. These include the Wentzel-Kramers-Brillouin (WKB) approximation (*10*), Rayleigh-Ritz, power-series expansion, and finite-element methods. For a SI fiber with its constant refractive index core, one can obtain closed-form analytic results from the scalar wave equation for the case of cylindrical symmetry (*1*):

$$\frac{1}{r}\frac{d}{dr}\left(r\frac{dR}{dr}\right) + \left[n(r)^2 k_0^2 - \beta^2 - \frac{\nu^2}{r^2}\right]R = 0 \tag{19}$$

where $n(r)$ is the refractive index, ν is the azimuthal mode number (a non-negative integer), and $R(r)$ is the scalar component of the electric field.

We probed the index profile of a SI POF at high resolution by measuring the differential mode delay time (DMD), which is highly sensitive to extremely small feature sizes in the index profile (*11*). DMD measures the time delays of small guided mode groups launched down the fiber from specified launch angles at the fiber input end (*12*). The DMD as a function of normalized mode number (m/M) is shown in Fig. 1B for a typical SI POF sample. The calculated index profile for the SI POF is $n_f = 1.492 \pm 0.001$ (for $r < 480$ μm) and $n_c = 1.420 \pm 0.004$ (for $r > 480$ μm). On the basis of these results, the analytical equations yield a calculated bandwidth of 27 ± 3 MHz for a fiber length of 100 m, which also agrees with the results from WKB approximation and finite element analysis. However, this value differs by a factor of 3 from the experimentally measured bandwidth of 80 ± 10 MHz for 100 m (Fig. 1C) (*13*). We attribute the bandwidth difference between the measured value of 80 MHz and the profile-determined value of 27 MHz to strong mode coupling that effectively increases the bandwidth.

A direct test for the presence of strong mode coupling is to measure the length dependence of the fiber pulse broadening, given as $\sigma \propto L^\alpha$. Again, in the strongly coupled regime where EMD is established, pulse broadening increases as the square root of length, rather than as the usual linear dependence. Figure 2A shows a log-log plot of the optical pulse broadening in a typical high-quality SI POF with a numerical aperture (NA) of 0.51 versus the fiber length of <50 m for four different launching conditions. A least-squares fit yields $\alpha = 0.99 \pm 0.01$ for NA = 0.12 and $\alpha = 0.97 \pm 0.02$ for NA = 0.25. These results indicate that for these underfilled launching conditions, the pulse broadening is essentially a linear function of fiber length and the system is in the weakly coupled limit. In contrast, when the light is coupled in with a high-NA launch and most of the mode volume is excited, the length dependence of the pulse broadening shows two distinct regions in Fig. 2A. In the first region, a least-squares fit yields $\alpha = 0.97 \pm 0.03$ for NA = 0.40 and $\alpha = 0.96 \pm 0.10$ for NA = 0.65, indicating that mode coupling is far from complete. In the second region, the measured data indeed exhibit strong mode coupling behavior, with pulse broadening slowing down markedly and the fit producing $\alpha = 0.54 \pm 0.01$ for NA = 0.40 and $\alpha = 0.57 \pm 0.01$ for NA = 0.65, near the ideal value of $\alpha = 0.5$. The results demonstrate good agreement between theory and experiment.

The coupling length L_c, which marks the crossover from weakly to strongly coupled regimes, is ~15 m (Fig. 2A). Furthermore, from the length dependence of pulse broadening, the ratio of the bandwidths in the presence and absence of strong mode coupling is related to the coupling length L_c and propagation length L through the expression

$$\sqrt{\frac{L}{L_c}} = \frac{B_{wc}}{B_{w0}} \qquad (20)$$

where B_{wc} and B_{w0} are the bandwidths in the presence and in the absence of strong mode coupling, respectively. This relation, combined with the calculated bandwidth of 27 ± 3 MHz, gives the predicted bandwidth of ~70 ± 8 MHz for a fiber length of 100 m, in agreement with the experimental value of 80 ± 10 MHz for 100 m.

Additional evidence of strong mode coupling is given by far-field radiation patterns of SI POF (*9*). Figure 2B shows angular scans of the far-field intensity under a variety of launch conditions for a typical SI POF with NA = 0.51 (*14*). For each experiment, light was launched into the fiber at a specified input angle with respect to the fiber axis. When light was launched into the fiber under high-NA conditions, the output distribution consisted of a disk, regardless of the incident angle, which demonstrates that mode coupling is complete and the EMD condition is achieved.

Measurements of the length dependence of the far-field intensity revealed the crossover from strongly coupled to weakly coupled regimes in SI POF. As the fiber was cut back toward the coupling length L_c with all other conditions remaining the same, angular scans of the fiber output at first became increasingly sensitive to the launch angle, indicating that light propagation was starting to stray from EMD. At shorter lengths near L_c and below, a sharp, distinct ring was observed at high scanning angles (Fig. 2C) that arose from a weakly coupled condition in which only a group of higher order modes were excited. Mode coupling was no longer complete under these conditions.

The transition from disk to ring in far-field patterns with increasing launch angle provides a method for determining the strength of the mode coupling. Following from Eq. 16, the transition angle θ_t is related to the fiber length L and coupling coefficient d_0 through the relation

$$\log \theta_t = \frac{1}{2} \log L + \log 2D^{1/2} \qquad (21)$$

(*9*). In a log-log plot of the measured transition angle as a function of fiber length (shown with a least-squares fit in Fig. 3), the slope is 0.53 ± 0.01, demonstrating good agreement between theory and experiment. From Eq. 17, the coupling coefficient d_0 is found to be $1.09 \pm 0.02 \times 10^4$ m^{-1}. The coefficient d_0 for POFs is about two orders of magnitude larger than that typically found for GOFs; hence the L_c for POF is much shorter than that for GOF.

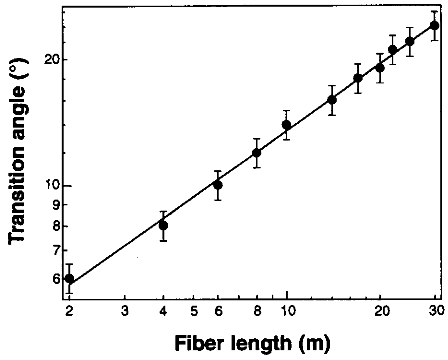

Fig. 3. Log-log plot of transition angle as a function of fiber length (L) (solid circles) and least-squares fit (solid line) following Eq. 21, with $D = 0.562 \pm 0.008 \times 10^{-3}$ from Eq. 21.

Mode Coupling in Graded-Index Plastic Optical Fiber

A GI POF provides a multimode waveguide in which modal dispersion is compensated by both mode coupling and the graded index (*7, 8*). The GI profile is formed by interfacial gel polymerization in a solid preform before fiber melt drawing (*15*). The interfacial gel method relies on selective diffusion of a low–molecular weight monomer together with heavier dopant molecules of higher refractive index in a polymer gel phase. The final material diffusion profile is fixed spatially by complete polymerization of the monomer, resulting in a graded refractive index profile. However, the resulting index profile for a typical polymethylmethacrylate (PMMA)-based GI POF sample (Fig. 4A) is only partially graded, even though GI POFs consistently exhibit multigigahertz bandwidth performance. From fast Fourier transforms of measured output pulses (Fig. 1C), the bandwidth was determined to be 3.0 ± 0.4 GHz for a fiber length of 100 m. As described below, the enhanced bandwidth is due to mode coupling arising from random perturbations in the core index.

Detailed analysis of the GI profile requires DMD fiber measurements. The DMD as a function of fiber radial position is shown in Fig. 4B for a typical GI POF sample. The important feature is that the DMD profile shows the fiber core containing two major optical regions. Starting from the fiber center ($r = 0$), the central core region extends over $0 < r < r_1$. The second region is the core-cladding

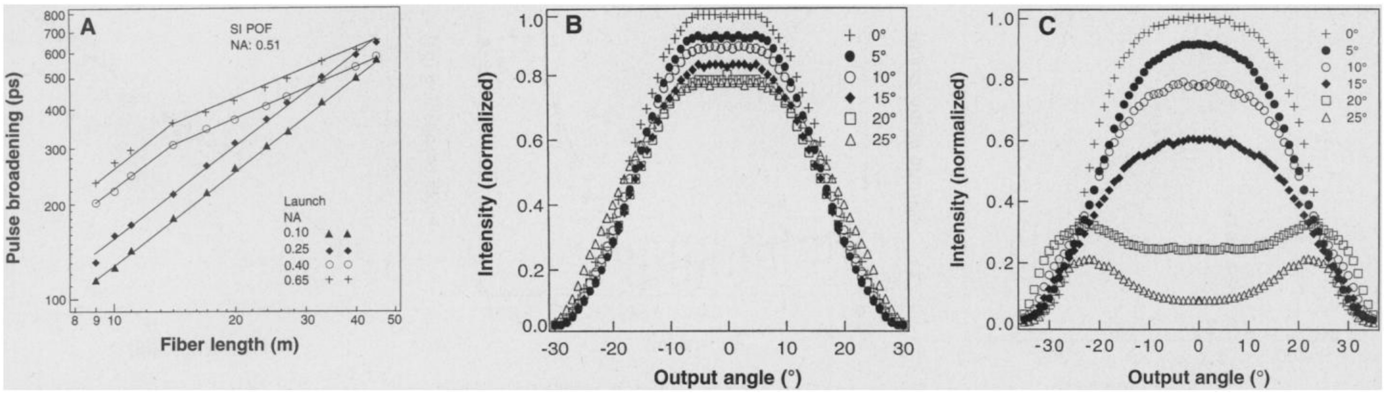

Fig. 2. (**A**) Log-log plot of pulse broadening as a function of fiber length (L) at different launching numerical apertures (NA) for SI POF sample and least-squares fit (solid lines) to $\sigma \propto L^{\alpha}$ (*7*). The pulse broadening (σ) is determined by $\sigma = (\tau_1^2 - \tau_2^2)^{1/2}$, where τ_1 and τ_2 are the FWHM of the light source and fiber output, respectively. (**B**) Far-field radiation disk patterns from a 30-m SI POF (NA = 0.51) when a collimated light beam was launched into the fiber with a high-NA (0.40) microscope objective. Symbols denote different angles between the center of the incident light beam and the fiber axis (*7*). (**C**) Far-field radiation patterns for a 10-m SI POF in the weakly coupled regime, showing characteristic ring formation at 20° and 25° input angle (*7*).

region, ranging over $r_1 < r < a$. The central core region maintains a negative slope with increased fiber radial position. Thus, the outer modes travel faster than the inner modes, indicating that the refractive index profile in this region overcompensates the modal dispersion. In the core-cladding region, the DMD exhibits a positive slope throughout, and modal dispersion is undercompensated in this region.

The DMD data were used to analyze the index profile, which is approximated with multi-α values as

$$n(r) = \sqrt{n_f^2 - (n_f^2 - n_c^2)\left(\frac{r}{a_i}\right)^{\alpha_i}} \qquad (22)$$

where n_f and n_c are fixed in the fitting process, and i denotes each index profile section delineated by the DMD data. Figure 4A demonstrates good agreement between the experimentally measured index profile and that calculated from Eq. 22. The index profile contains two broad, optically distinct regions of central core ($0 < r < r_1$) and of core cladding ($r_1 < r < a$). The central core is near parabola-like with an α value near 2, whereas the core-cladding region connects steeply to the cladding, reminiscent of low-bandwidth multimode SI fiber with a large α value.

The DMD profile reveals direct evidence of mode coupling caused by random index perturbations in the core. In approaching the cladding boundary, the experimental data turn over from a large positive slope to one that is nearly flat. This important feature is further made evident in analysis of the DMD profile calculated from the index profile through the WKB approximation,

$$m(\beta,k_0) = \int_0^{r_2} [n^2(r)k_0^2 - \beta^2]r\,dr \qquad (23)$$

$$\tau = \frac{1}{c}\frac{d\beta}{dk_0} = -\frac{1}{c}\left(\frac{\partial m/\partial k_0}{\partial m/\partial\beta} + \frac{\partial m/\partial n_f}{\partial m/\partial\beta}\frac{dn_f}{dk_0} + \frac{\partial m/\partial n_c}{\partial m/\partial\beta}\frac{dn_c}{dk_0}\right) \qquad (24)$$

where m is the number of modes above the propagation constant β, τ is the group delay time, and r_2 is determined by $n(r_2) = \beta/k_0$. The solid curve in Fig. 4B is the resulting calculated DMD profile for guided modes and stands in good agreement with experiment, especially for lower order modes in the central core region. That the lower order modes are not severely affected by mode coupling is explained by the index profile in this region, which is nearly parabolic with a small α value. Hence, following Eq. 13, only a narrow, sparse spectrum of perturbations is available to induce mode coupling. In contrast, the index profile in the core-cladding region is step-like with a large α value and, as a result, from Eq. 13, there is a much more broad and dense spectrum of perturbations for mode coupling. In this second region, the measured positively sloped DMD turned over to a nearly flat profile, resulting in a large divergence between the calculated and measured group delay times for the outermost guided modes. The outer modes are the most highly dispersive, having a large influence on the observed fiber bandwidth. By coupling and mixing with high–group velocity inner modes, the group delay times of the outer modes are markedly reduced, and the observed pulse broadening is thus effectively decreased.

The pulse broadening represented by the impulse response function $h(\tau)$ is calculated from the measured refractive index profile and group delay time τ in the WKB approximation,

$$h(\tau) = p(m)\left|\frac{dm}{d\tau}\right| \qquad (25)$$

where $p(m)$ is the modal power distribution, which is determined by differential mode attenuation measurements. The equations assume that mode coupling is not present. The bandwidths calculated from the Fourier transform of the impulse response function $h(\tau)$ for different GI POF samples are always nearly an order of magnitude smaller than the measured bandwidths. Thus, for example, the calculated bandwidth for the fiber sample of Fig. 4A is only 0.43 GHz for a length of 100 m, whereas the measured value is 3.0 ± 0.4 GHz for 100 m.

As in the case of SI POF, the presence of strong mode coupling in GI POF is clearly evident in the dependence of pulse broadening on fiber length, given as $\sigma \propto L^\alpha$. A log-log plot of the experimentally determined pulse broadening as a function of fiber length is given in Fig. 4C for a typical GI POF sample, along with a least-squares fit. The measured data indeed exhibit strong mode coupling behavior with the experimental value $\alpha = 0.6$, close to the ideal strong coupling limit of $\alpha = 0.5$ and far from the weak coupling linear dependence of $\alpha = 1$.

The coupling length L_c of GI POF is relatively short, near 2 m, as calculated from Eq. 20. The relatively short coupling lengths for SI POF and GI POF contrast markedly with the kilometer-long coupling lengths characteristic of GI GOF. The shorter coupling lengths L_c in POF, together with the large magnitude measured for the mode coupling coefficient d_0, reflect intrinsic large fluctuations in density and concentration in addition to the usual extrinsic random perturba-

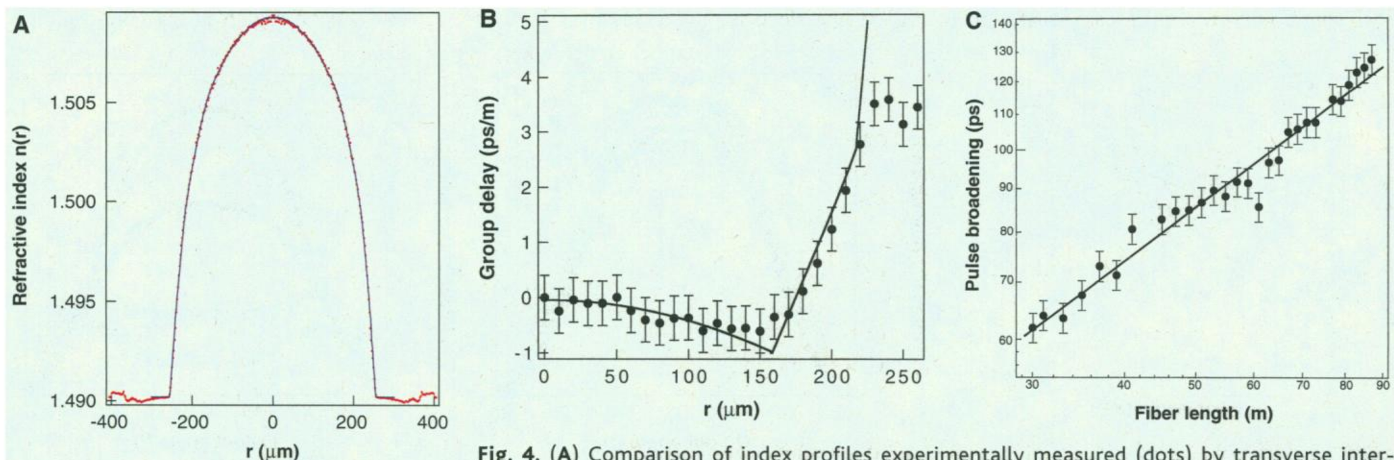

Fig. 4. (**A**) Comparison of index profiles experimentally measured (dots) by transverse interferometric method (8) and calculated from Eq. 22 (solid curve) with a_1 = 346.3 µm, α_1 = 2.06 for $0 < r < 157$ µm; a_2 = 273.1 µm, α_2 = 2.96 for 157 µm $< r <$ 217 µm; and a_3 = 254.5 µm, α_3 = 4.26 for 217 µm $< r <$ 255 µm. (**B**) Comparison of measured differential mode delay normalized to length as a function of the fiber scanning position (r) for a PMMA-based GI POF (dots) and calculated differential mode delay profile (solid curve) from multi-α profile by Eqs. 23 and 24. (**C**) Log-log plot of pulse broadening as a function of fiber length for a typical PMMA-based GI POF doped with benzyl benzoate (solid circles) and least-squares fit (solid line) to $\sigma \propto L^\alpha$ (8), with $\alpha = 0.6 \pm 0.1$.

tions (such as microbends) responsible for mode coupling. The presence of the material perturbations is consistent with the comparatively low glass transition temperatures observed in POF materials (*16*).

In summary, high-speed fiber optic networks increasingly require high-performance fiber links in short-distance (~100 m) applications such as LANs and FTTD (*17*). Existing network systems, such as asynchronous transfer mode (ATM) and Ethernet, can operate at several hundred megabits per second and provide upgrade paths to 1 gigabit per second and greater. Current high-performance, short-distance fiber links are multimode doped silica glass optical fibers with a graded refractive index. Primarily because of its attractive ductile properties and light weight, multimode plastic optical fiber in SI and GI forms is also being considered, especially for very short (<50 m) quick-connect applications (*18*). We have found that mode coupling in plastic optical fiber is a basic mechanism for achieving high bandwidth performance.

References and Notes

1. D. Marcuse, *Principles of Optical Fiber Measurements* (Academic Press, New York, 1981).
2. ———, *Bell Syst. Tech. J.* **48**, 3187 (1969).
3. S. Kawakami and T. Nishizawa, *IEEE Trans. Microwave Theory Tech.* **MTT-16**, 814 (1968).
4. S. D. Personick, *Bell Syst. Tech. J.* **50**, 843 (1971).
5. D. Marcuse, *ibid.* **52**, 817 (1973).
6. D. Gloge, *ibid.* **51**, 1767 (1972).
7. G. Jiang, R. F. Shi, A. F. Garito, *IEEE Photonics Tech. Lett.* **9**, 1128 (1997).
8. R. F. Shi, C. Koeppen, G. Jiang, J. Wang, A. F. Garito, *Appl. Phys. Lett.* **71**, 3625 (1997).
9. W. A. Gambling, D. A. Payne, H. Matsumura, *Electron. Lett.* **9**, 412 (1973).
10. See, for example, T. Okoshi, *Optical Fibers* (Academic Press, New York, 1982).
11. D. Marcuse, *Theory of Dielectric Waveguides* (Academic Press, New York, 1974).
12. Differential mode delay measurements in POFs were performed in the time domain using a temperature-stabilized InGaAlP laser diode that produced 45-ps pulses at 660 nm (peak power, 10 mW) at a repetition rate of 2 MHz. The laser diode output was collimated by a GRIN lens, spatially filtered, and then collimated by a 15-cm (focal length) lens that was focused onto the fiber end by another 15-cm lens. The focused beam spot was ~5 μm in diameter. To excite only a small group of guided modes in the fiber, we kept the launch NA of the light beam focused into the fiber below 0.007, which is much less than the POF NA. The GI POF sample was mounted on a motorized stage, with its input end face normal to the incident beam, and translated across the beam for selective mode excitation at specified radial positions. Similarly, in the case of SI POFs, the fiber sample input end was rotated. The fiber output was detected by a sampling optical oscilloscope, and the data were stored and analyzed on a laboratory computer. The group delay for each pulse was obtained by averaging over the entire pulse.
13. The bandwidth performance of an optical fiber can be determined by measuring either the impulse response in the time domain or the spectral response in the frequency domain. In our experiments, we measured the impulse response of POF samples in the time domain using a picosecond laser diode with a high repetition rate. In our current setup, with τ_1 and τ_2 the full widths at half maximum (FHWM) of the light source and output signals of the fiber, respectively, the impulse response at the FWHM of the fiber is given by $\sigma = (\tau_1^2 - \tau_2^2)^{1/2}$. Fast Fourier transforms were carried out for accurate bandwidth measurements. The light source was a temperature-stabilized InGaAlP laser diode capable of producing 45-ps pulses at 660 nm wavelength. The repetition rate of the laser diode could be as high as 2 MHz. The laser diode output was first collimated by a GRIN lens and then spatially filtered. It was then collimated by a 15-cm lens and focused onto the POF by a micro objective lens. The output light signal was detected by a sampling optical oscilloscope. The time delay of the trigger signal for the optical oscilloscope could be adjusted by the delay box as well as by the diode controller. The main part of the optical oscilloscope consisted of a sampling streak tube to convert the light incident on the photocathode into photoelectrons. The photoelectrons were sampled and then directed to a phosphor screen, where they were converted to light. The light was then detected by a photomultiplier tube. The data stored in the oscilloscope could be fed into a computer for further data analysis. The time resolution of the system is better than 10 ps.
14. After being modulated by a chopper, the light was focused onto the input end of the fiber mounted on a rotation stage, which allowed the launch angle to be varied with respect to the fiber axis. The output end of the fiber was mounted at the center of another rotation stage. Angular scans of the far-field intensity were made using a silicon photodiode with a small active area of 1 mm, which was set on an arm that could rotate around the output fiber end. The photodiode and the fiber end were 15 cm apart, so the angular resolution was better than half a degree. The electrical signal from the photodiode was sent to a lock-in amplifier referenced by the chopper.
15. Y. Koike, T. Ishigure, E. Nihei, *IEEE J. Lightwave Technol.* **13**, 1475 (1995). Currently, new advanced fabrication methods are under development in several laboratories worldwide.
16. L. L. Blyler, C. S. Koeppen, H. E. Bair, in *POF Asia-Pacific Forum '96*, 10 and 11 December 1996, Tokyo, Japan (POF Consortium, Tokyo, 1996), pp. 58–61.
17. P. E. Green Jr., *IEEE J. Select. Areas Commun.* **14**, 764 (1996).
18. T. Kaino, in *Polymers for Lightwave and Integrated Optics*, L. Hornak, Ed. (Dekker, New York, 1992), pp. 1–38.

19. Supported by the Defense Advanced Research Projects Agency (grant F49620-94-1-0468), the U.S. Air Force Office of Scientific Research, and the Pittsburgh Supercomputing Center. We gratefully acknowledge the contributions of R. F. Shi and G. Jiang.